Electronic Supplementary Material (ESI) for

Peculiarly fast Li-ion conduction mechanism in a succinonitrile-based molecular crystal electrolyte: a molecular dynamics study

Ryoma Sasaki,[*a,b] Makoto Moriya,[c,d] Yuki Watanabe,[a] Kazunori Nishio,[a] Taro Hitosugi,[a] and Yoshitaka Tateyama[*a,b]

[a] *School of Materials and Chemical Technology, Tokyo Institute of Technology, Tokyo 152–8552, Japan*

[b] *Center for Green Research on Energy and Environmental Materials (GREEN) and International Center for Materials Nanoarchitectonics (MANA), National Institute for Materials Science (NIMS), Ibaraki 305–0044, Japan*

[c] *Department of Science, Graduate School of Integrated Science and Technology, Shizuoka University, Shizuoka 422–8529, Japan*

[d] *College of Science, Academic Institute, Shizuoka University, Shizuoka 422–8529, Japan*

* E-mail: sasaki.r.ak@m.titech.ac.jp

* E-mail: TATEYAMA.Yoshitaka@nims.go.jp

Table of Contents

S1. Relationship between various defects and Li-ion diffusivity

We investigated the relationship between various defects and Li-ion diffusivity in $Li\{N(SO_2F)_2\}(NCCH_2CH_2CN)_2$ ($Li(FSA)(SN)_2$). Four models were considered.

(1) Perfect-crystal model consisting of a perfect-crystalline structure (108 Li + 108 FSA + 216 SN).

(2) Li-vacancy model consisting of a crystalline structure with one Li-ion removed (107 Li + 108 FSA + 216 SN).

(3) FSA-vacancy model consisting of a crystalline structure with one Li-ion removed (108 Li + 107 FSA + 216 SN).

(4) Li-interstitial model consisting of a crystalline structure in which one Li-ion is added to a suitable interstitial site (109 Li + 108 FSA + 216 SN), as shown in **Fig.** S1(a).

Fig. S1(b) shows the Li-ion mean-square displacements (MSDs) of the above-mentioned models. The MSD exhibiting the largest change with time was along the *c*-axis in the Li-ion vacancy model. This result demonstrates that the conduction of $Li(FSA)(SN)_2$ is anisotropic, and that the conduction is predominantly promoted by the Li-ion vacancies along the *c*-axis.

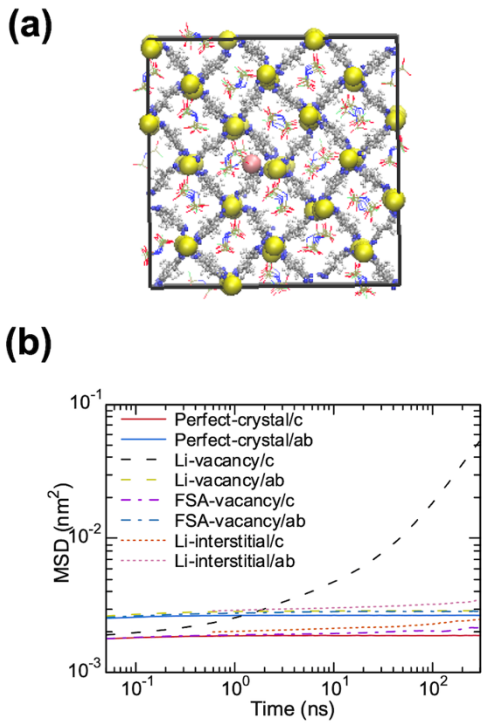

Fig. S1. (a) Snapshot of the Li-ion interstitial model. The pink atom is the interstitial Li-ion. (b) Li-ion MSDs as a function of time in the Li-ion vacancy, Perfect-crystal, FSA-ion vacancy, and Li-ion interstitial models. The notation in the graph takes the form of "Model" / "direction (*c*-axis or *ab*-plane)".

S2. Calculation of the Li-ion self-diffusion coefficient

We calculated the self-diffusion coefficient using the slope of the MSD, as shown in Eq. (1):

$$D = \lim_{t\to\infty}\left[\frac{1}{2dt}\mathrm{MSD}(t)\right] \quad (1)$$

where d is the dimension of diffusion (= 1 along the c-axis) and t is the time. There are two problems in calculating the slow Li-ion diffusion promoted in the single Li-ion vacancy model. First, there are only five Li atoms acting as carriers in the defective c-axis channel. As a result, a considerable sampling is required to reach statistical convergence. Second, high temperature simulations cannot be applied to organic crystals because of their low melting temperatures. Therefore, many steps are required to reach the diffusive regime. Owing to these limitations, we performed long simulations on the order of microseconds. The MSD in the diffusive regime is proportional to t^1 (MSD(t) $\propto t^1$). In other words, the onset of the diffusive regime (t_{diff}) occurs when the slope of the log-log plot of MSD(t) is 1. We determined the values of t_{diff} and self-diffusion coefficient, as shown in **Figs. S2** and **S3**. The MSD(t_{diff}) is approximately 0.26 nm^2 = (5.1 Å)^2, which is consistent with the Li hopping distance along the c-axis. Further, we obtained the self-diffusion coefficient by fitting MSD(t) from t_{diff} to the time of arrival of the MSD at 1.0 nm^2. We also checked for the convergence of the arrival time of the MSD at 0.26 and 1.0 nm^2.

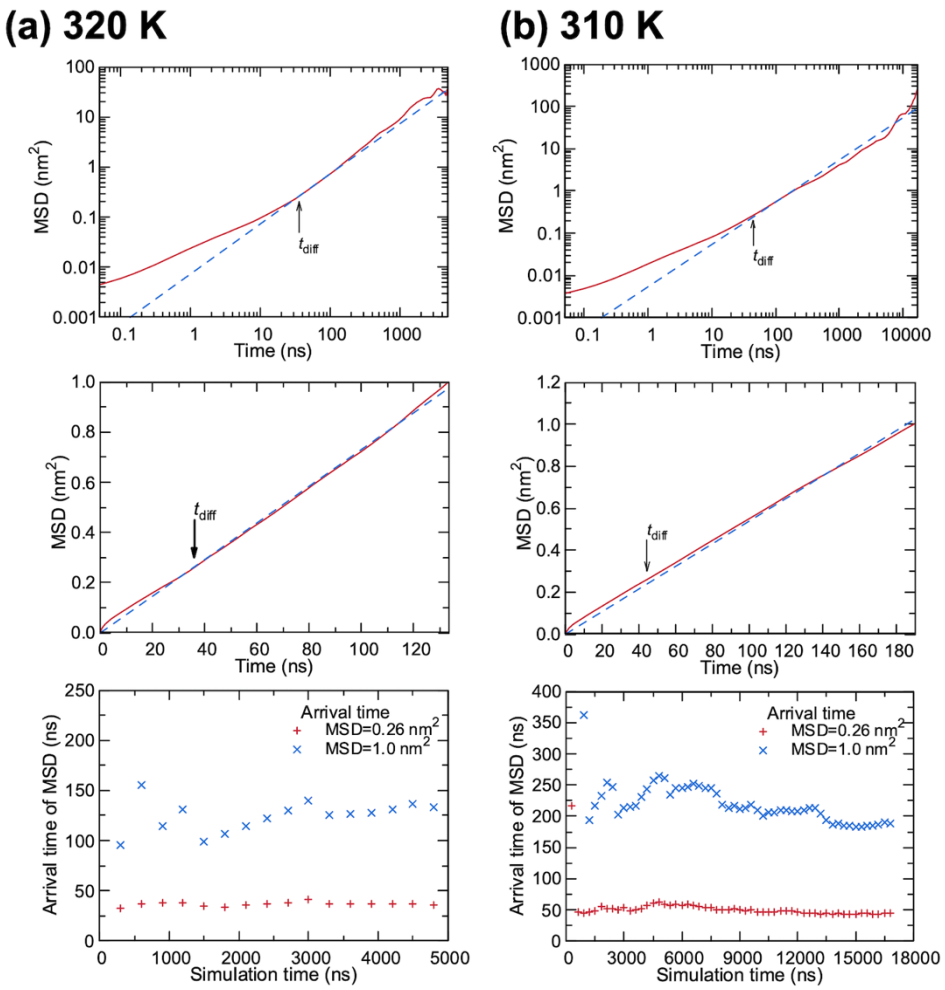

Fig. S2. Log-log plots of Li-ion MSDs in the defective channel, MSDs and fitting lines, and the arrival times when the MSDs reach 0.26 nm^2 and 1.0 nm^2 at (a) 320 K and (b) 310 K.

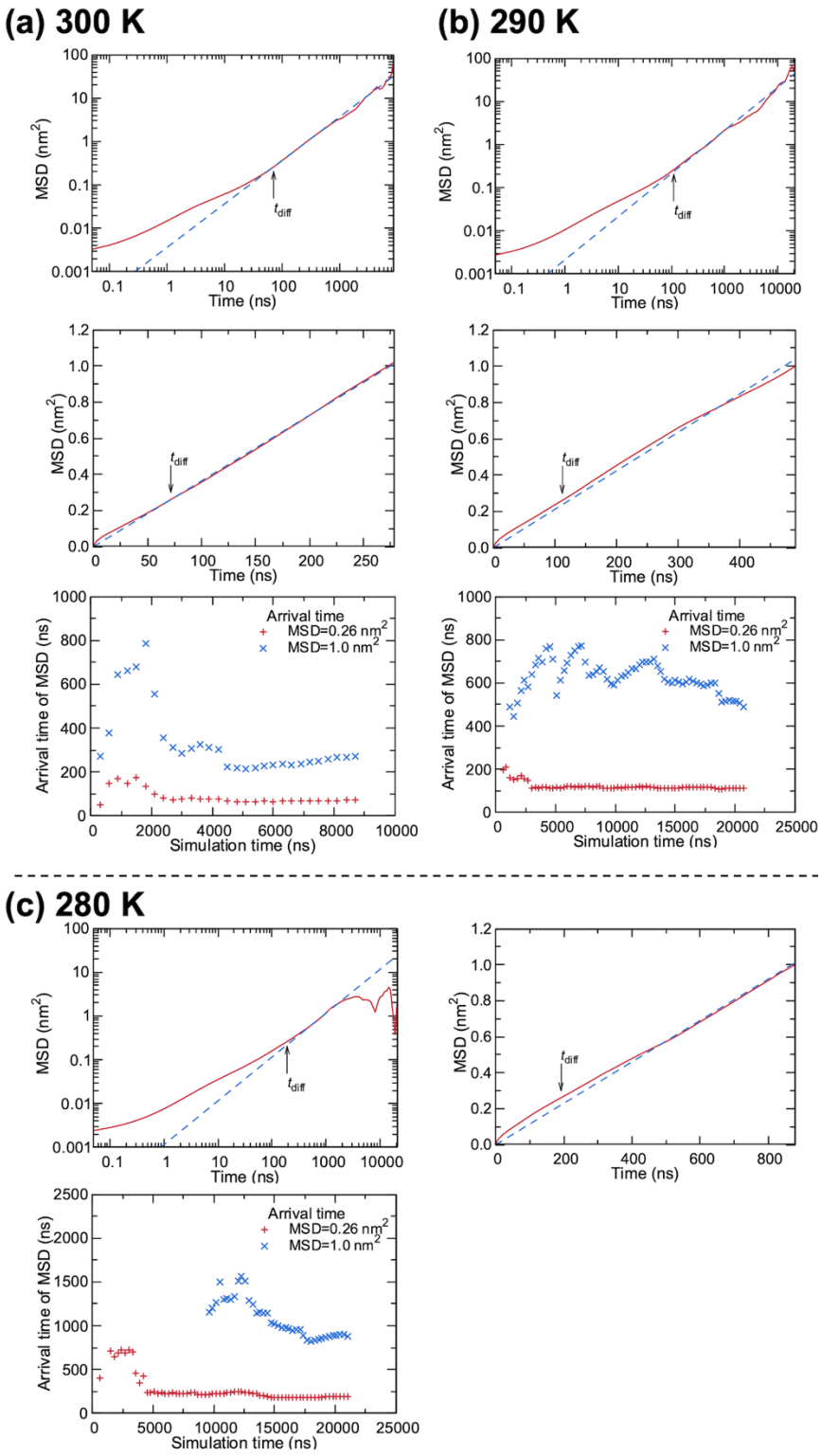

Fig. S3. Log-log plots of Li-ion MSDs in the defective channel, MSDs and fitting lines, and the arrival times when the MSDs reach 0.26 nm^2 and 1.0 nm^2 at (a) 300 K, (b) 290 K, and (c) 280 K.

S3. Differences among GAFF2, Rigid-dihedral force field (FF), and All-trans FF

The function of the second generation of the general AMBER force field (GAFF2)[1] is expressed by the following equations:

$$E_{\mathrm{MM}} = \sum_{\text{bonds}} k_b(r - r_0)^2 + \sum_{\text{angles}} k_\theta(\theta - \theta_0)^2 + \sum_{\text{dihedrals}} k_d[1 + \cos(n_{\mathrm{d}}\varphi - \delta)] + \sum_{\text{impropers}} k_i(\chi - \chi_0)^2 + \sum_{i<j} \frac{q_i q_j}{4\pi\varepsilon_0 r_{ij}} + \sum_{i<j} 4\,\varepsilon_{ij}\left[\left(\frac{\sigma_{ij}}{r_{ij}}\right)^{12} - \left(\frac{\sigma_{ij}}{r_{ij}}\right)^{6}\right] \quad (2)$$

The torsional potential ($E_{\mathrm{torsion}}(\varphi)$) as a function of the dihedral angle of NC-C-C-CN (φ) in GAFF2 is given by:

$$E_{\mathrm{torsion}}(\varphi) = k_{\mathrm{d1}}[1 + \cos(n_{\mathrm{d}}\varphi - \delta_{\mathrm{d1}})] + k_{\mathrm{d2}}[1 + \cos(n_{\mathrm{d2}}(\varphi + 120\,^\circ) - \delta_{\mathrm{d2}})] + E^{\mathrm{ff}} \quad (3)$$

where $\{k_{\mathrm{d1}}, n_{\mathrm{d1}}, \delta_{\mathrm{d1}}\}$ and $\{k_{\mathrm{d2}}, n_{\mathrm{d2}}, \delta_{\mathrm{d2}}\}$ are the force field parameters of the dihedral angle d1 (C1-C3-C3-C1) and d2 (HC-C3-C3-HC) in **Fig. S4**, respectively. E^{ff} represents the other force field terms that are dependent on φ. To obtain a desirable potential profile, we prepared new force field parameters $\{k_{\mathrm{d1}}, n_{\mathrm{d1}}, \delta_{\mathrm{d1}}\}$ and $\{k_{\mathrm{d2}}, n_{\mathrm{d2}}, \delta_{\mathrm{d2}}\}$ for the rigid–dihedral and all-trans FFs. The modified FF parameters are listed in **Table S1**.

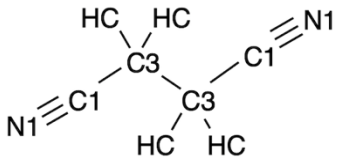

Fig. S4. Atom types for $NCCH_2CH_2CN$ (succinonitrile; SN).

Table S1. Force field parameters of dihedral angles d1 (C1-C3-C3-C1) and d2 (HC-C3-C3-HC).

Force Field	k_{d1} (kJ mol^{-1})	n_{d1}	δ_{d1} (°)	k_{d2} (kJ mol^{-1})	n_{d2}	δ_{d2} (°)
GAFF2	0.65084	3	0	0.50208	3	0
Rigid-dihedral FF	3.25422	3	0	0.50208	3	0
All-trans FF	0.65084	3	0	21.42208	1	0

S4. Chemical structure of fumaronitrile

The candidate which we proposed as a dopant for the Li(FSA)SN_2 molecular crystal is fumaronitrile (**Fig. S5**).

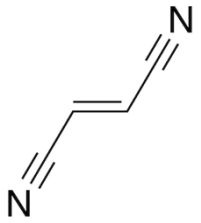

Fig. S5. Chemical structure of fumaronitrile (N≡C–CH=CH–C≡N).

References

(1) Case, D. A.; Ben-Shalom, I. Y.; Brozell, S. R.; Cerutti, D. S.; Cheatham III, T. E.; Cruzeiro, V. W. D.; Darden, T. A.; Duke, R. E.; Ghoreishi, D.; Gilson, M. K.; Gohlke, H.; Goetz, A. W.; Greene, D.; Harris, R.; Homeyer, N.; Huang, Y.; Izadi, S.; Kovalenko, A.; Kurtzman, T.; Lee, T. S.; LeGrand, S.; Li, P.; Lin, C.; Liu, J.; Luchko, T.; Luo, R.; Mermelstein, D. J.; Merz, K. M.; Miao, Y.; Monard, G.; Nguyen, C.; Nguyen, H.; Omelyan, I.; Onufriev, A.; Pan, F.; Qi, R.; Roe, D. R.; Roitberg, A.; Sagui, C.; Schott-Verdugo, S.; Shen, J.; Simmerling, C. L.; Smith, J.; SalomonFerrer, R.; Swails, J.; Walker, R. C.; Wang, J.; Wei, H.; Wolf, R. M.; Wu, X.; Xiao, L.; York, D. M.; Kollman, P. A. Amber 2018. University of California: San Francisco 2018.